

## Letter to the Editor

# HI in the galactic halo

P.M.W. Kalberla<sup>1</sup>, G. Westphalen<sup>1</sup>, U. Mebold<sup>1</sup>, Dap Hartmann<sup>2</sup>, and W.B. Burton<sup>3</sup>

<sup>1</sup> Radioastronomisches Institut der Universität Bonn, Auf dem Hügel 71, D-53121 Bonn, Germany

<sup>2</sup> Center for Astrophysics, 60 Garden Street, Cambridge, MA 02138, USA

<sup>3</sup> Sterrewacht Leiden, P.O. Box 9513, RA 2300 Leiden, The Netherlands

Received 3 December 1996 / Accepted 6 March 1998

**Abstract.** We find solid evidence for diffuse HI gas at substantial  $z$  heights in our Galaxy, with a velocity dispersion of  $\sigma = 60 \text{ km s}^{-1}$  and a vertical projected column density of  $N_{\text{HI}} = 1.4 \cdot 10^{19} \text{ cm}^{-2}$ . This pervasive component of the emission spectrum could be identified in the Leiden/Dwingeloo 21-cm Survey (LDS) after increasing the accuracy further by correcting the observations for reflections from the ground. Investigations of receiver bandpass and stray radiation effects could not explain this component as an artifact of the instrumentation.

Assuming that the distribution of mass and pressure perpendicular to the galactic plane is in hydrostatic equilibrium with the galactic potential, we derive a vertical exponential scale height of  $h_z \simeq 4.4 \text{ kpc}$  for the observed diffuse high-dispersion HI component. The radial distribution is characterized by the corresponding galactocentric scale length  $A_1 \simeq 15 \text{ kpc}$ .

**Key words:** Galaxy: halo – Galaxy: kinematics and dynamics – radio lines: ISM

### 1. Introduction

The detection of neutral interstellar clouds at large  $z$  distances (Münch 1957) led to the hypothesis of a gaseous galactic halo (Spitzer 1956). A rarefied high-temperature ionized gas ( $T \simeq 10^6 \text{ K}$ ) was assumed to be in pressure equilibrium with normal interstellar clouds. A relatively cool neutral halo ( $T \simeq 10^4 \text{ K}$ ) was postulated by Pikelner & Shklovsky (1958). Their model predicted emission lines of neutral species with velocity dispersions of  $70 \text{ km s}^{-1}$  due to turbulent motions, but was abandoned a few years later because such lines were not observed.

Observations of faint, wide lines originating from a galactic halo are plagued by considerable instrumental difficulties. Instrumental improvements in recent years have led to increasing evidence for emission from a neutral galactic halo. HI gas with dispersions of up to  $35 \text{ km s}^{-1}$  has been found in the directions of the galactic poles by Kulkarni & Fich (1985). Lockman & Gehman (1991) pointed out that the turbulent energy of these HI clouds can support layers up to distances  $z > 1 \text{ kpc}$ . Evidence

for an extended neutral galactic halo was presented by Albert et al. (1994). Diffuse high-dispersion HI gas was found in sensitive observations of extragalactic objects by Schulman et al. (1994). In 10 out of 14 deep integrations of face-on galaxies HI profile wings were detected and interpreted as due to gas with dispersions of  $30$  to  $50 \text{ km s}^{-1}$ .

This interpretation implies galactic halo gas of modest ( $T \lesssim 10^4 \text{ K}$ ) temperatures. However, spectral line observations of highly ionized atoms indicate temperatures of  $T \simeq 10^5 \text{ K}$  (Savage et al. 1997), while a plasma with  $T \simeq 10^{6.3} \text{ K}$  is required to explain the soft X-ray background (Kerp 1994, Pietz et al. 1998). This implies that the galactic halo gas cannot be assigned a single temperature.

We have analyzed the Leiden/Dwingeloo 21-cm Survey (LDS) and found high velocity dispersion (HVD) HI emission widely distributed over the sky. In Sect. 2 we describe the observations and present our findings. In Sect. 3 we discuss instrumental difficulties and demonstrate that our results seem unaffected by such problems. In Sect. 4 we reproduce our observations by a model HI distribution. A discussion is given in Sect. 5.

### 2. Observations and data analysis

The LDS (Hartmann 1994, Hartmann & Burton 1997) is the first large-scale 21-cm line survey which has been corrected for stray radiation from the side- and back-lobes of the antenna pattern (Hartmann et al. 1996). We have further improved the quality of the LDS data by correcting the observations for spurious line emission caused by radiation reflected from the ground into the receiver (details are given in Sect. 3).

Fig. 1 shows profiles averaged over all longitudes and over  $10^\circ$  in latitude for  $b = 85^\circ$  (bottom) to  $b = 5^\circ$  (top). To avoid any systematical biases due to southern sky data missing in the LDS, Fig. 1 was restricted to positive galactic latitudes. Weak, extended profile wings are visible which cannot be seen in individual profiles due to the noise (typically  $50 \text{ mK}$  after Hanning smoothing). Differential galactic rotation causes the wings to get broader at lower latitudes.

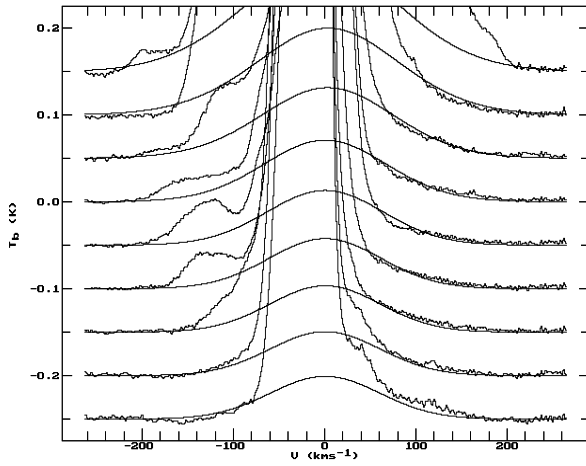


**Fig. 1.** Profiles from the Leiden/Dwingeloo Survey (LDS) covering all positive galactic latitudes, corrected for ground reflections and averaged over all galactic longitudes and over  $10^\circ$  in latitude. The bottom profile is centered at  $b = 85^\circ$ , the top one at  $b = 5^\circ$ . The zero levels of subsequent profiles are spaced by 50 mK. The solid lines follow from the model discussed in Sect. 4, corresponding to the emission of a co-rotating HI halo with a vertical scale height of  $h_z = 4.4$  kpc and a radial scale length of  $A_1 = 15$  kpc.

The properties of the profile wings have been studied by Westphalen (1997) who averaged the LDS in boxes of  $10^\circ \times 10^\circ$  and calculated the variance of the line emission for each velocity channel. The variance emphasizes small-scale spatial structure, instrumental problems, and interference. Thus the variance spectra can be used to test whether the wings are due to smooth emission. In Fig. 1 emission from HVCs and IVCs is clearly visible at negative velocities, superposed on the extended profile wings. At positive velocities the wings are only marginally affected by HVCs. These wings predominantly originate from gas which is smoothly distributed over large angular scales.

Averaged spectra for  $\sim 250$  different boxes have been decomposed into Gaussian components by fitting only those channels of the averaged spectra which were found to be uncontaminated by fluctuations. Thus the analysis was biased to be most sensitive to components of large angular extent. HVD HI lines were found in all of the averaged spectra. The mean velocity dispersion of these lines is  $\sigma = 60(\pm 3)$   $\text{km s}^{-1}$  at the north galactic pole and increases at lower latitudes (Fig. 3). Such an increase can be explained by Kolmogoroff turbulence. For a plane-parallel HI distribution the length of the line of sight increases as  $(\sin b)^{-1}$ . The velocity dispersion is then expected to vary as  $(\sin b)^{-1/3}$ . Thus  $\sigma = 60$   $\text{km s}^{-1}$  at the pole is consistent with the value  $\sigma \sim 80$   $\text{km s}^{-1}$  which we find at  $b = 25^\circ$ . The average line broadening due to differential galactic rotation in Fig. 3 is negligible ( $\lesssim 5\%$ ). At the north galactic pole the column density of this component is  $N_{\text{HI}} = 1.4(\pm 1) \cdot 10^{19}$   $\text{cm}^{-2}$ .

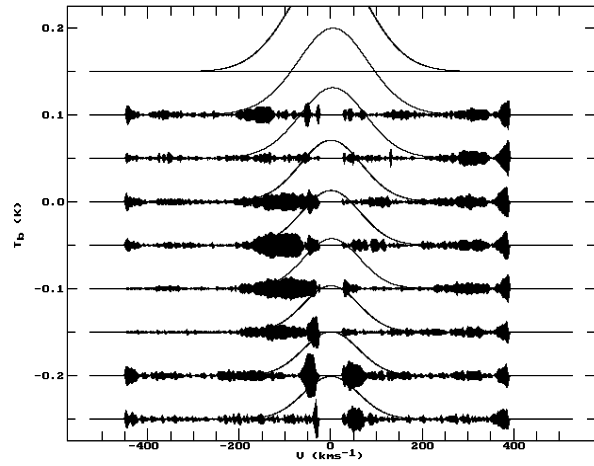


**Fig. 2.** Estimated baseline uncertainties of the profiles plotted in Fig. 1, derived after a re-analysis of the LDS database. Observations affected by interference have been excluded from the inter-comparison. Only the range  $|v_{\text{lsr}}| > 25$   $\text{km s}^{-1}$  and  $b > 10^\circ$  is given. The emission corresponding to the halo model (see Sect. 4) is plotted for comparison. Unlike Fig. 1, the full velocity ranges included in the analysis are plotted here.

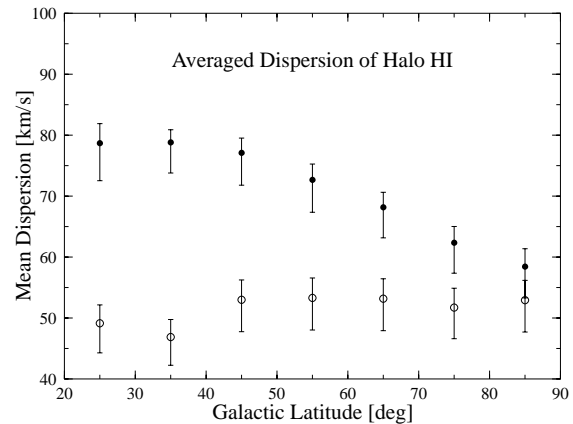


**Fig. 3.** The mean velocity dispersion of the diffuse high velocity dispersion (HVD) component ( $\bullet$ ) and of the stray radiation ( $\circ$ ) as a function of galactic latitude.

### 3. The reliability of observed HI lines

The profiles shown in Fig. 1 need further investigation concerning possible problems associated with instrumentation and data processing. It must be excluded that any spurious intensities would result from the baseline correction or from the stray-radiation correction procedure.

We repeated the reduction of the LDS to check whether the procedures (described by Hartmann 1994) could be responsible for the observed HVD components. In the LDS reduction, third-order baselines had been fitted to emission-free parts of the spectra (Hartmann 1994, Sect. 2.3.4). Additionally, partial baselines had been fitted and subtracted, as had sine-wave ripples (assumed to be caused by standing waves between the telescope dish and receiver).

It seemed conceivable that the removal of partial baselines had produced artifacts which could be interpreted as an HVD component. In repeating the reduction we therefore did not subtract any partial baselines. For the determination of emission-free line channels we introduced additional constraints. For each box of pointed observations within an area of  $5^\circ \times 5^\circ$  we calculated the variance of the signal. All channels showing fluctuating lines were eliminated from the emission-free regions. Thus any emission which varies noticeably with position (clouds) or time (interference) was suppressed. After elimination of the obvious line emission around  $v_{\text{lsr}} \simeq 0 \text{ km s}^{-1}$  we excluded an additional range of  $30 \text{ km s}^{-1}$  at both wings of the line from the emission-free regions. Excluding unreliable channels at the edges of the bandpass, we fitted a third-order baseline over the velocity range  $-430 \text{ km s}^{-1} < v_{\text{LSR}} < 380 \text{ km s}^{-1}$ . Sine-wave ripples were eliminated in a similar way as described by Hartmann (1994).

To exclude any possible software problems, the code for the entire reduction procedure was rewritten. The data reduction process was iterated several times to find optimum boundary conditions for the baseline determinations. For the majority of the observations, good baselines could be achieved this way. However, severe interference caused a number of profiles to fail the fitting routine regardless of the boundary conditions.

To identify profiles which were affected by interference we used the recorded temperature  $T_{\text{SYS}}$  of the 21-cm receiver. Abnormally high or low  $T_{\text{SYS}}$  values (by  $\gtrsim 25\%$ ) were assumed to indicate bad observations. We rejected all observations for which fluctuations in  $T_{\text{SYS}}$  exceeded 10% of the running mean. In addition we rejected all profiles with an rms-noise exceeding the average noise by a factor of 4, as well as those affected by interference spikes with amplitudes exceeding the noise by a factor of 10. Profiles which passed these criteria were found to have well-defined baseline regions free of line emission. On average the baseline was defined by 417 channels, corresponding to 50% of the analyzed velocity range. Due to our restrictions  $\sim 28\%$  of the observations were excluded from the analysis.

As mentioned in Sect. 2, systematic spurious intensities due to reflections from the ground (Hartmann et al. 1996) limit the accuracy of the LDS. Such lines with dispersions  $\sigma \lesssim 30 \text{ km s}^{-1}$  and intensities up to  $\simeq 50 \text{ mK}$  affected the analysis of the profiles averaged over  $10^\circ \times 10^\circ$  predominantly between latitudes  $40^\circ \lesssim b \lesssim 70^\circ$  (Westphalen, 1997). Based on 2700 spectra showing the typical signature of reflections from the ground, a proper correction for such reflections was calculated and applied to the entire LDS data set. The first attempts to correct profiles for ground reflections by Hartmann et al. (1996) had failed because a significant fraction of the test profiles were affected by interference. This problem could be overcome as described above only after analyzing a large number of affected profiles for this purpose.

We further checked our data for additional systematic errors in the stray radiation correction. Any increase of a side- or back-lobe level did not affect the profile wings at the most extreme velocities, but only introduced significant errors in the velocity range of the main line components. We therefore compared the dispersions of stray-radiation profiles and HVD components.

Stray radiation profiles were decomposed into Gaussian components using the same criteria as for the analysis of corrected profiles. Forcing the broadest component to fit the extreme profile wings we found that the dispersion of the stray radiation components is significantly smaller than the HVD components identified in the corrected profiles.

Fig. 3 shows the average velocity dispersions of the broadest stray radiation components which were removed from the spectra, along with the dispersions observed in the averaged profiles. Not only are the stray-radiation velocity dispersions systematically smaller than those of the HVD component, they are uncorrelated with galactic latitude. The latitude dependence of the HVD component is the strongest evidence that this emission is genuine. The systematic uncertainties due to residual stray radiation are estimated to be  $\sim 5\text{-}15 \text{ mK}$ , well below the  $\gtrsim 50 \text{ mK}$  amplitude observed for the HVD component.

The data obtained after such a restrictive reduction as described above are incomplete, but in an unbiased manner, and can be used to estimate the uncertainties which may have affected the profiles plotted in Fig. 1. No preference can be given to neither the original dataset nor the revised version (both corrected for reflections from ground). Thus positive or negative deviations have the same probability. The uncertainties estimated this way are plotted in Fig. 2 for  $|v_{\text{lsr}}| > 25 \text{ km s}^{-1}$ . No comparison can be made for latitudes  $b < 10^\circ$  since in this range the reliability of the baselines may be affected by extended wings of the conventional HI emission. We rejected profiles for which less than 300 channels were used to fit the baseline. To allow a comparison with the model calculations given in Sect. 4, we have also plotted the model data in Fig. 2. The amplitudes of the model exceed 50 mK while the baseline-uncertainties of the analyzed averaged profiles are at most 15 mK. We conclude that our data reduction leads essentially to the same results as the reduction by Hartmann (1994). The correction for reflections from ground is essential for an analysis of weak lines. Residual errors in the stray radiation corrections are probably in the range 10 to 20 mK, hence too small to affect the HVD components found in all latitudes.

#### 4. Hydrostatic equilibrium model

We interpret the low-intensity profile wings at the extreme velocities as emission from neutral gas in hydrostatic equilibrium with the gravitational potential of the Galaxy. The density distribution  $n(z)$  of the HI halo gas is then due to the balance between the turbulent pressure of the HVD component and the gravitational potential  $\Phi(z)$ :

$$n(z) \propto \exp[-\Phi(z)/(c \cdot \sigma^2)]$$

$c$  is a constant defined by the vertical scale height,  $\sigma$  is the HVD velocity dispersion, and  $\Phi(z)$  is the gravitational potential as given by Kuijken & Gilmore (1989). From the column density of the HVD component in direction to the north galactic pole we obtain the constraint  $\int n(z) dz = 1.4 \cdot 10^{19} \text{ cm}^{-2}$ .

We model the distribution  $n(R, z)$  of the halo gas throughout the Galaxy following the approach of Taylor & Cordes (1993), separating radial and horizontal dependencies:  $n(R, z) =$

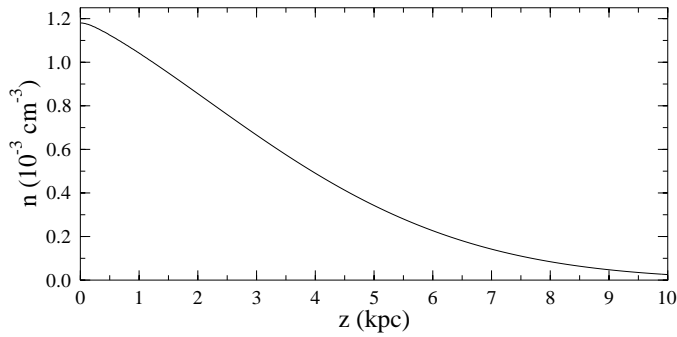


**Fig. 4.** Vertical distribution  $n(z)$  of the HI halo gas in the solar vicinity as derived from our model calculations.

$g_1(R) \cdot n_0 \cdot \exp[-\Phi(z)/(c \cdot \sigma^2)]$  where  $n_0 = n(R_\odot, 0)$  is the mid-plane density and  $g_1(R) = \text{sech}^2(R/A_1)/\text{sech}^2(R_\odot/A_1)$  defines the radial density distribution;  $R_\odot = 8.5$  kpc.

We modeled the emission of HI halo gas corresponding to such a distribution for various scale lengths  $h_z$  and  $A_1$ , assuming that the halo gas is co-rotating with the disk. The rotation curve was taken from Fich et al. (1990). The best fit to the observations is given in Fig. 1 for the scale lengths  $h_z = 4.4$  kpc and  $A_1 = 15$  kpc. This result yields a value of  $c=3$ , implying a halo model where gas, magnetic fields and cosmic rays are in pressure equilibrium. Fig. 4 shows the corresponding distribution  $n(z)$ .

## 5. Results and discussion

The accuracy of the LDS has been improved by eliminating intensities received as reflections from ground. The emission at  $\sim 250$  positions after averaging over  $10^\circ \times 10^\circ$  was decomposed into Gaussian components. We find evidence for large-scale galactic HI emission with a velocity dispersion of  $60 (\pm 3)$  km s $^{-1}$  and a column density of  $N_{\text{HI}} = 1.4 (\pm 1) \cdot 10^{19}$  cm $^{-2}$  projected to the north galactic pole. Assuming that this gas is co-rotating with the disk, the observed extended wings in the profiles can be modeled. The  $n(R, z)$  distribution is characterized by a hydrostatic equilibrium with a mid-plane density  $n_0 = 1.2 (\pm 0.2) 10^{-3}$  cm $^{-3}$  in the solar vicinity. The exponential scale height is  $h_z = 4.4 (\pm 0.3)$  kpc, the radial scale length is  $A_1 = 15 (\pm 5.0)$  kpc.

Our analysis implies that HI gas due to its turbulent pressure remains an important constituent of the halo at  $z > 1$  kpc. In particular the scale height of the Reynolds layer (880 pc, Taylor & Cordes 1993) is exceeded considerably. On the other

hand, halo gas at temperatures of  $T \simeq 10^{6.3}$  K is needed to explain the soft X-ray background (Kerp 1994). Pietz et al. (1998) modeled the X-ray background in the 1/4 and 3/4 keV range and concluded that the X-ray halo is defined by the *same* model parameters as given in Sect. 4. This implies, that the galactic halo has a multi-phase composition with temperatures ranging from  $10^4$  to  $10^{6.3}$  K. Transition regions between these phases may exist, as indicated by highly ionized gas at intermediate temperatures. It appears plausible to assume that the highly ionized gas components in the halo share the turbulent properties of the HI gas. This conclusion is supported by Savage et al. (1997) who found turbulent velocities of  $\sim 60$  km s $^{-1}$  for the Cvi lines. They derive a scale height of  $h(\text{Cvi}) = 4.4 (\pm 0.6)$  kpc which is in excellent agreement with the HI scale height derived here. We conclude that the highly ionized gas components must be intermixed with HI gas as analyzed in this letter.

*Acknowledgements.* We thank the referee, H. van Woerden, for his critical analysis concerning possible problems with the data reduction. This initiated a complete reanalysis of the LDS observations. We are grateful to J. Lockman, J. Kerp, J. Pietz, K.S. de Boer and W. Hirth for helpful discussions.

## References

- Albert, C.E., Welsh, B.Y., Danly, L. 1994, ApJ 437, 204.
- Fich, M., Blitz, L., Stark, A.A. 1990, ApJ 342, 272.
- Hartmann, D. 1994, PhD thesis, University of Leiden.
- Hartmann, D., Burton, W.B. 1997, Atlas of Galactic Neutral Hydrogen, Cambridge University Press.
- Hartmann, D., Kalberla, P.M.W., Burton, W.B., Mebold, U., 1996, A&AS 119, 115.
- Kerp, J., 1994, A&A 289, 597.
- Kuijken, K., Gilmore, G. 1989, MNRAS 239, 605.
- Kulkarni, S.R., Fich, M. 1985, ApJ 289, 792.
- Lockman, F.J., Gehman, C.S. 1991, ApJ 382, 182.
- Münch, G. 1957, ApJ 125, 42.
- Pietz, J., Kerp, J., Kalberla, P.M.W., Burton, W.B., Hartmann, D., Mebold, U., 1998, A&A 332, 55.
- Pikelner S.B., Shklovsky I.S., 1958, IAU Symposium 8, Reviews of Modern Physics, 30, 935.
- Savage, B.D., Sembach, K.R., Lu, L., 1997, AJ 113, 2158.
- Schulman, E., Bregman, J.N., Roberts, M.S. 1994, ApJ 423, 180.
- Spitzer, L. 1956, ApJ 124, 20.
- Taylor, J.H., Cordes, J.M. 1993, ApJ 411, 674.
- Westphalen, G., 1997, PhD thesis, University of Bonn.